

Position Sensors for LISA Drag Free Control

**William J. Weber^{1,2,3,†}, Antonella Cavalleri⁴, Rita Dolesi^{1,2},
Giorgio Fontana⁵, Mauro Hueller^{1,2}, and Stefano Vitale^{1,2,3}**

1. Università di Trento, Dipartimento di Fisica, I-38050, Povo (TN), Italy
2. Istituto Nazionale di Fisica Nucleare (INFN), Sezione di Padova
3. Consorzio Criospazio Ricerche (CCR)
4. Centro Fisica dello Stato Aggregato (CEFSA)
5. Università di Trento, Dipartimento di Ingegneria

Abstract. The extreme level of isolation from stray forces required for LISA makes the development of “drag free control” technologies essential to the mission. We report here on progress in the development of a capacitive, six degree of freedom, position sensor designed to meet the required low levels of position readout noise ($1 \text{ nm}/\text{Hz}^{1/2}$) and stray force noise ($3 \times 10^{-15} \text{ N}/\text{Hz}^{1/2}$) across the LISA bandwidth of .1 mHz to .1 Hz. In this paper we briefly discuss sensor design and expected performance before presenting preliminary noise measurements made with a prototype sensor.

PACS numbers: 4.80.Nn, 7.87.+V, 6.30.Bp

1. Introduction

At low frequencies the sensitivity of LISA (Laser Interferometry Space Antenna) is expected to be limited by stray forces acting on the test masses serving as “end mirrors” for a long baseline ($5 \times 10^6 \text{ km}$) Michelson interferometer [1]. A flat force noise spectral density, $S_f^{1/2}$, results in a very “red” $\frac{1}{\omega^2}$ displacement noise (and thus measured gravitational wave strain noise), which, for the LISA target goal of $3 \times 10^{-15} \text{ N}/\text{Hz}^{1/2}$, is expected to dominate the LISA noise below 1 mHz.

A “drag free control” system to shield a test mass from external forces consists of a satellite driven by precision thrusters to remain centered around the test mass, according to a relative position sensor. The essential task is to perform the position measurement and control with a minimum of force applied to the test mass, allowing it to fall as freely as possible in the external gravitational field.

In a high gain drag free control loop, the residual force on the test mass is

$$f_{res} = f_{str} + k_{int} \left(x_n + \frac{F_{str}}{k_{DF}} \right) \quad (1)$$

Here, f_{str} corresponds to any stray (position independent) forces acting on the test mass, including both (non-gravitational) unshielded external forces and those originating from the satellite itself. Noise in the spacecraft position (with respect to the test mass) arises from the sensor measurement noise x_n and the finite time response of the drag free control loop (with a force-to-displacement response k_{DF}) to

† To whom all correspondence should be addressed (weber@science.unitn.it)

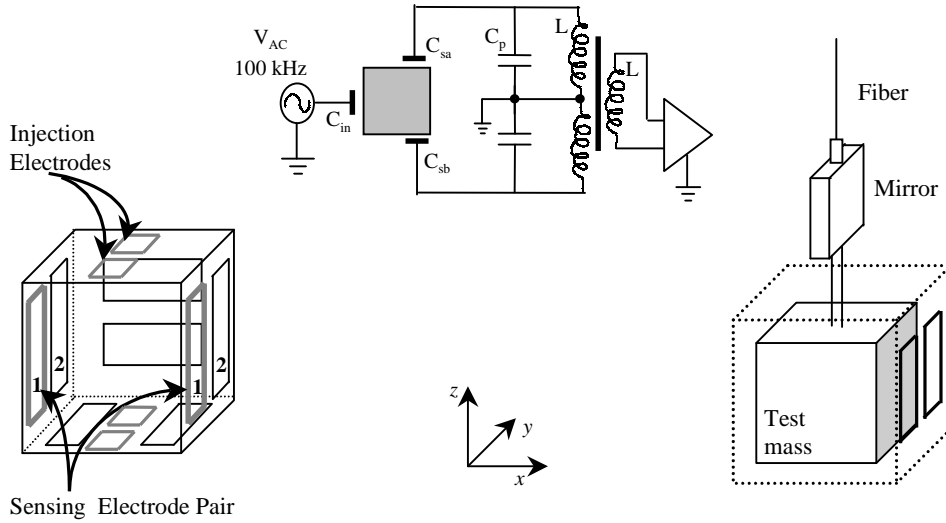


Figure 1. Schematic view of sensor housing (left), sensor bridge readout circuitry (center), and pendulum assembly (right).

forces acting on the spacecraft, F_{str} . This spacecraft position noise, multiplied by any internal satellite - test mass springlike coupling k_{int} , produces a force noise.

The position sensor needed for drag free control thus differs from standard high precision accelerometers in that it must minimize the total force acting on the test mass, f_{res} , rather than the position measurement noise, x_n . For capacitive position sensors, for example, this requires a tradeoff between the sensor noise, which decreases linearly with the applied sensing voltage, and the electrostatic coupling, k_{el} , which increases with the voltage squared. For LISA, position noise at the $\text{nm}/\text{Hz}^{1/2}$ level is acceptable [1], limiting forces arising from other satellite - test mass couplings which cannot be completely eliminated (gravitational, for instance).

We present here a LISA drag free sensor design approach and then a preliminary experimental evaluation of a prototype sensor noise performance. A ground based program to measure stray forces and force couplings associated with the sensor itself is also essential for the LISA mission (and the planned LISA Technology Demonstrator mission, LTP) and is discussed in another paper in these proceedings [2].

2. Sensor Design and Leading Sources of Force Noise

A prototype six degree of freedom capacitive position sensor used for the measurements presented here is shown schematically in Fig. 1. Detailed analyses of the design and resultant force noise have been presented elsewhere [3, 4]. As such, we highlight here just a few major differences from other precision space accelerometer designs [5, 6]:

- **Geometry** The cubic sensor shown at left in Fig. 1 detects test mass displacement by the modulated separation in the capacitances between the test mass and sensing electrodes (C_s), with each of the six opposing pairs of electrodes

forming a differential capacitive-inductive bridge, resonated at $\omega_0 \approx 2\pi \times 100$ kHz (see circuit diagram). The same electrodes can also be used to apply electrostatic forces needed to stabilize the test mass at low frequencies and along the non-measurement degrees of freedom[4]. Signal combination yields all translational and rotational displacements, with, for instance, the sum of channels 1 and 2 giving the test mass x translation and their difference the rotation about the z -axis. Cubic symmetry is broken along the z -axis by the presence of smaller electrodes (C_{in}) which inject an AC current through the test mass. Design symmetry limits the effect of force cross-coupling between the different degrees of freedom.

- **Gap Size** Relatively large capacitance gaps ($d = 2\text{mm}$, resulting in $C_s \approx 2.2$ pF), are chosen in order to avoid a class of difficult to model couplings which decrease quickly with the electrode - test mass separation. These include test mass charging and patch charge effects[7], both of which produce couplings decreasing as $\frac{1}{d^3}$.
- **Materials** A high thermal conductivity metal-ceramic construction is chosen here over materials, such as ULE, typically used in accelerometers for their high thermal stability (the sensor prototype used here is made of Aluminum with Macor dielectric spacers, while a higher precision Molybdenum / Shapal model is currently being prepared for study). Here, instead of eliminating thermal expansion to reduce position noise, the idea is to limit forces, from radiation pressure and radiometric effects, arising from thermal gradients across the sensor, which impose stricter thermal environment constraints than the $1 \text{ nm/Hz}^{1/2}$ position noise requirement.

2.1. Intrinsic Sensor Performance

The aim of this design is to prevent surface, thermal, and cross-talking effects from dominating over the well understood thermal sensor readout noise and the electrostatic force coupling arising from the sensor bias voltage. The intrinsic readout noise, for a single translational channel, arising from the finite quality factor Q of the resonant bridge circuitry and dominated by losses in the differential transformer, has spectral density

$$S_x^{1/2} = \frac{d}{\sqrt{\omega_0}} \left[\frac{4k_B T}{C_s V_M^2} \frac{1}{2Q\omega_0^2 LC_s} \right]^{1/2} \quad (2)$$

The sensor AC bias is thus increased until the test mass voltage V_M is large enough to bring sensor noise comfortably below $1 \text{ nm/Hz}^{1/2}$. The product of this position noise with the electrostatic readout coupling, $k_{el} = \frac{C_s V_M^2}{d^2}$, results in force noise

$$S_f^{1/2} = k_{el} S_x^{1/2} = \frac{4k_B T}{S_x^{1/2} \omega_0} \frac{1}{2\omega_0^2 LC_s Q} \quad (3)$$

For the sensor dimensions and circuitry currently used [4], Eqn. 3 corresponds to a force noise of roughly $10^{-16} \text{ N/Hz}^{1/2}$, well below the LISA limit. Significant force noise contributions also arise from circuit noise “back-action” and the low frequency electrostatic suspension. However, Eqn. 3 gives a rough magnitude of the intrinsic sensor disturbance level. One could further reduce this force coupling noise by reducing the sensing gap to increase C_s , but, repeating, the conservative approach adopted here is to prevent other effects associated with small gaps from dominating over this nominal level.

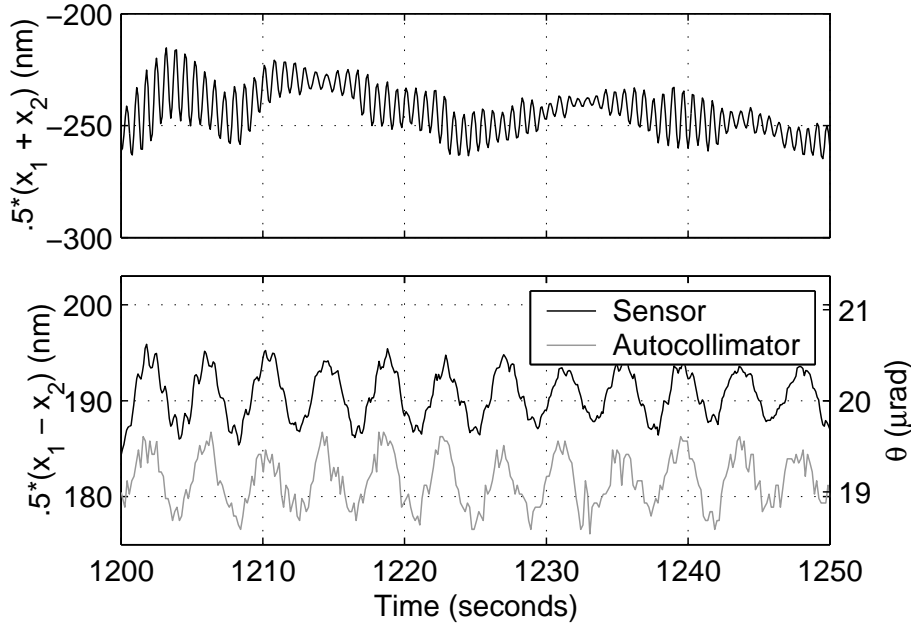


Figure 2. Time series of sensor translational (top) and rotational (bottom) signals. Note that the differential signal, $\frac{x_1 - x_2}{2}$, shown with the autocollimator readout, is the rotational angle θ multiplied by half the 19mm on-center electrode separation.

3. Experimental Details

Measurements were performed with two pairs of electrodes (1 and 2 in Fig. 1) with signals from each channel's bridge circuitry read out by lock-in detection and combined offline to yield both translational and rotational displacement. The test mass is hung by a rigid aluminum bar, which enters the sensor through a hole on the top electrode plate and is suspended by a 23 mm long, 100 μm diameter tungsten wire. A mirror mounted on the bar permits an independent optical autocollimator readout of the test mass rotation. The resultant structure has simple and torsional pendulum modes at, respectively, 1.4 and .24 Hz. The data presented here are measured in air, with a torsion pendulum quality factor of roughly 110.

Sensor calibration is performed by first moving the sensor translationally, with the micropositioner stage on which it is mounted, in order to determine the ratio of the two channel sensitivities, which is critical for the signal recombination. Then, with the pendulum excited torsionally, the two channel outputs are compared against the autocollimator signal to calibrate the absolute sensitivity. Figure 2 displays a typical time series of sensor data, including a comparison with the autocollimator angular data, which demonstrates the simple and torsional pendulum modes and sensor resolution at the nm level.

In addition to permitting calibration with test mass motion, the short pendulum has several advantages for characterizing sensor performance. The relatively stiff torsion constant of the short, thick fiber translates into a thermal torsional noise

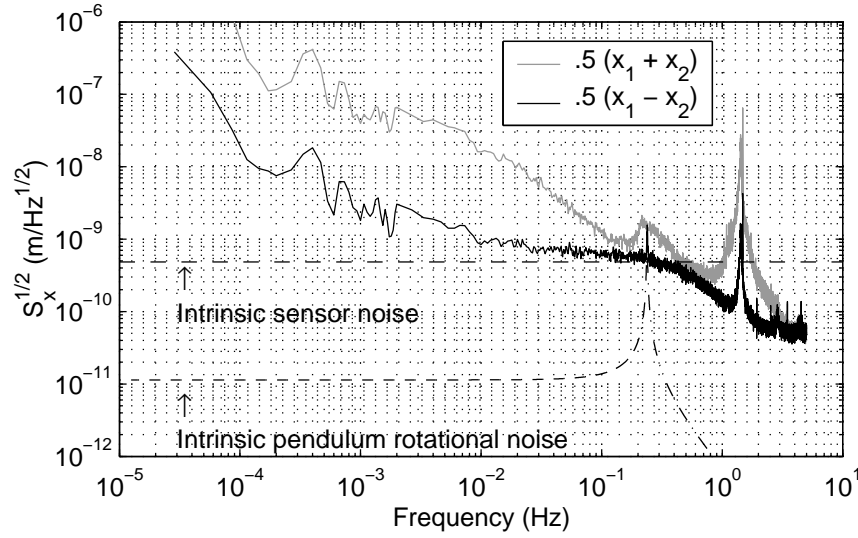


Figure 3. Sensor translational and rotational noise plotted against the sensor intrinsic electronic thermal noise and the torsion pendulum intrinsic mechanical rotational noise.

that is well below the ideal noise floor of the sensor (except very close to the torsional resonance frequency), and thus there is the possibility to measure the sensor rotational noise with a “still” test mass. The sensor housing can be centered about the test mass to zero the sensor at the μm level, in order to minimize the effect of noise sources proportional to the signal level, such as amplitude noise in the AC bias source. Finally, the pendulum, sensor, and bridge electronics are integrated inside a dedicated vacuum torsion pendulum facility which, with the substitution of a longer (≈ 1 m) and thinner ($25 \mu\text{m}$) fiber, will permit measurement of weak forces exerted on the test mass by the sensor.

4. Experimental Sensor Noise Data and Discussion

Figure 3 displays the translational ($\frac{x_1+x_2}{2}$) and rotational ($\frac{x_1-x_2}{2}$) noise spectral densities for roughly 10 hours of sensor data measured with the pendulum setup. The translational data reflects the simple pendulum susceptibility to seismic noise, floor tilt, and thermal distortion in the pendulum suspension, resulting in translational noise well above that expected for the sensor, including a broad peak near .2 Hz observed elsewhere[8] and associated with oceanic activity. Note that the magnitude of the simple pendulum peak at 1.4 Hz is not quantitatively accurate, as it is attenuated by the 300 ms low pass filter used in these measurements.

While the translational data characterize the environmental disturbances more than the sensor itself, the torsional motion has a higher immunity to such disturbances, allowing the rotational data to provide a significant upper limit on sensor noise. Above 10 mHz, the rotational noise is below $1 \text{ nm/Hz}^{1/2}$, within a factor of two of the theoretical sensor thermal readout noise, corresponding to a roughly 2 dB noise figure at high frequencies (this also corresponds to the voltage noise measured across the

whole LISA bandwidth with the sensor bias turned off). As such, the pendulum rotational noise is visible at frequencies near the .24 Hz torsional resonant frequency, where the noise level slightly exceeds the intrinsic thermal fluctuation noise. At lower frequencies, the measured noise climbs above the intrinsic level, to 4 nm/Hz^{1/2} at 1 mHz and to roughly 20 nm/Hz^{1/2} at .1 mHz.

Understanding the source of excess noise at low frequencies is critical to the evaluation of the sensor design. Because the signal levels are small (means displacements of order 1 μ m for each electrode pair), parametric noise due to fluctuations in oscillator amplitude or resonant circuitry gain cannot explain the observed noise. Likewise, measured bridge instabilities from the differential transformers should not contribute at this level. The temperature measurements are dominated by their own readout noise at the relevant frequencies (this has been since been improved and will be used to correlate sensor noise in future runs), but the upper limit on temperature fluctuations makes thermal distortion or thermal circuit gain fluctuations unlikely as a significant noise source. The low frequency noise in the autocollimator readout is below that of the capacitive sensor, and thus most of the excess low frequency noise in the sensor readout should not be attributed to true pendulum rotational noise.

The most plausible source of the observed excess rotational sensor noise is error in the relative calibration of the two channels. A slight error in measuring the ratio of the two channel sensitivities results in an imperfect signal combination, and thus the rather large level of test mass translational noise can “leak” into the rotational signal. This can be seen in Fig. 3 in the clear correlation between the translational and rotational spectra, which would imply a roughly 5% error in the ratio of the channel sensitivities. Indeed, one can artificially adjust this ratio to significantly improve the rotational noise, such that it is below 2 nm/Hz^{1/2} down to .5 mHz. While we calibrate the sensitivity ratio to better than 1% (at the beginning or end of a 15 hour run), long term fluctuations in this value at the several percent level are consistent with the resonant circuitry temperature sensitivity to the lab thermal environment. A more quantitative study of the relationship between the sensor gain and temperature should allow us to correct for the effect and to prevent the contamination of the sensor rotational noise data by translational mass motion.

5. Conclusion

The discussed position sensor design stresses the importance of lowering force noise at the expense of displacement sensitivity. Still, it is essential to reach, and demonstrate, the LISA position noise specification of 1 nm/Hz^{1/2}. A relatively high frequency torsion pendulum has been used to characterize the sensor’s rotational displacement noise, demonstrating compliance with the LISA target down to 10 mHz. We are currently working towards a full characterization of sensor noise performance at the nm/Hz^{1/2} level down to the LISA lower frequency limit of .1 mHz.

References

- [1] *LISA: A Cornerstone Mission for the Observation of Gravitational Waves*. ESA-SCI(2000)11. System and Technology Study Report
- [2] Hueller M, Cavalleri A, Dolesi R, Vitale S, and Weber W J (2001 Amaldi Meeting, to be published)
- [3] Cavalleri A, Dolesi R, Fontana G, Hueller M, Turneaure J, Vitale S, and Weber W 2001 *Class. Quantum Grav.* **18** 4133

- [4] *Drag Free Satellite Control* ESTEC contract #13691/99/NL/FM(SC) Final Report
- [5] Touboul P, Rodriques M, Willemot E, and Bernard A 1996 *Class. Quantum Grav.* **13** A67
- [6] Keiser G M, Buchman S, Bencze W, and DeBra D B 1998 *Proc 2nd Int. LISA Symp.* ed Folkner W
AIP Conf. Proc. **456** 188
- [7] Speake C C 1996 *Class. Quantum Grav.* **13** A291
- [8] Losurdo *et al* 1999 *Rev. Sci. Inst.* **70** 2507